Journal Pre-proofs

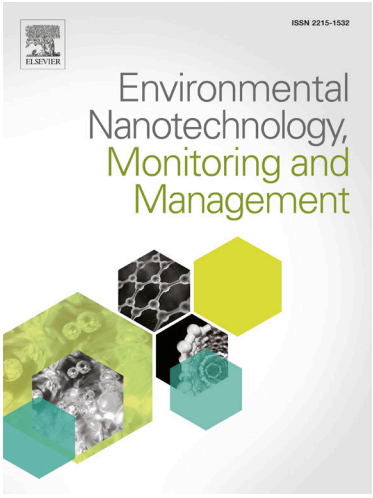

Morphology modulation of silica mesoporous nano- and microparticles for atrazine - controlled release

Federico Fookes, Carlos Busatto, María Eugenia Taverna, Natalia Casis, Maia Lescano, Diana Estenoz

PII: S2215-1532(22)00072-1
DOI: https://doi.org/10.1016/j.enmm.2022.100712
Reference: ENMM 100712

To appear in: *Environmental Nanotechnology, Monitoring & Management*

Received Date: 25 February 2022
Revised Date: 29 April 2022
Accepted Date: 9 June 2022

Please cite this article as: F. Fookes, C. Busatto, M. Eugenia Taverna, N. Casis, M. Lescano, D. Estenoz, Morphology modulation of silica mesoporous nano- and microparticles for atrazine - controlled release, *Environmental Nanotechnology, Monitoring & Management* (2022), doi: https://doi.org/10.1016/j.enmm.2022.100712

Morphology modulation of silica mesoporous nano- and microparticles for atrazine - controlled release

Federico Fookes,[a] Carlos Busatto,[a] María Eugenia Taverna,[a,b,c] Natalia Casis[a,c],Maia Lescano,[a] Diana Estenoz[a,c]

[a]INTEC (Universidad Nacional del Litoral – Conicet). Güemes 3450, (3000) Santa Fe, Argentina

[b]UTN Facultad Regional San Francisco, Av. de la Universidad 501, (2400) San Francisco, Argentina

[c]Facultad de Ingeniería Química, Santiago del Estero 2829, (3000) Santa Fe, Argentina

Abstract

Atrazine is a moderately toxic triazine, used as a selective pre- and post-emergence herbicide. After application, it remains in the environment due to its low biodegradability causing severe environmental effects. Several controlled release systems have been proposed in order to minimize the negative impact of the herbicide on the environment. In particular, mesoporous silica nanoparticles have shown great potential in the agricultural area due to their controlled size and porosity, high surface area and non-toxicity. In this work, silica nano- and microparticles were synthesized and evaluated as atrazine delivery systems. The morphology and size distribution of the particles were characterized using dynamic light scattering (DLS) and scanning electron microscopy (SEM). The release profiles were studied by *in vitro* assays in water. In addition, phytotoxicity tests were performed using *Lactuca sativa* seeds. The mesoporous nano- and microparticles exhibited sustained release for at least 24 h and reduced phytotoxicity compared to free atrazine.

Keywords: Silica; mesoporous nanoparticles; microparticles; atrazine

1. Introduction

Pesticides are chemical substances widely used in agriculture to increase the yield, improve the quality and extend the storage life of food crops.(Narenderan et al., 2020) According to the pest they control, pesticides can be classified as insecticides, herbicides, fungicides, rodenticides, nematicides among others. Between them, herbicides comprise about 47.5% of the pesticide annual global production, representing 0.95 million tons. They play a crucial role in agriculture in order to kill weeds following plant uptake by the leaves, stems, or roots.(de Albuquerque et al., 2020)

Atrazine (2-chloro-4-ethylamine-6-isopropylamine-s-triazine) is a synthetic herbicide used in several crops. This herbicide belongs to the persistent organic pollutants due to its low biodegradability and long half-life in water (between 30 and 100 days).(Runes et al., 2001) It has been estimated that after application, a large amount persists in the environment. Furthermore, due to its moderate water solubility (33 mg L^{-1}) and relatively low soil adsorption, atrazine can easily migrate into groundwater, representing a potential hazard to human health as this herbicide and its chlorinated metabolites are considered endocrine disruptors. Despite the related environmental drawbacks, atrazine is widely used in many countries including the United States, Brazil, China, and India. According to Alburqueque et al. (2020) about 24731 and 30000 tons of atrazine are commercialized in Brazil and the United States, respectively.(de Albuquerque et al., 2020)

In order to reduce the environmental toxicity of atrazine, several authors explored controlled release systems based on organic matrices including poly(epsilon-caprolactone)(Andrade et al., 2019; Clemente et al., 2014; Grillo et al., 2011; Pereira et al., 2014), lignin(Taverna et al., 2018), solid lipids(De Oliveira et al., 2015), poly(lactic acid-co-glycolic acid)(CHEN and Wang, 2019), among others. This technology allows the gradual release of the active principle over time with the aim of limiting the amount

immediately available for transport and degradation processes. In addition, it can help to extend the substance activity, reduce the residual amounts on foodstuffs, to save labor and energy by reducing the number of applications, as well as to increase safety for those applying pesticides.(Chevillard et al., 2012) The performance of the delivery systems based on organic matrix could be also controlled with the addition of inorganic clay fillers that improve the interaction with atrazine.(Jain et al., 2020) In addition, several works have reported the use of inorganic materials as matrices for atrazine controlled released including activated bentonites(Fernández-Pérez et al., 2004; Małyszka and Jankowski, 2004), anionic clays (Touloupakis et al., 2011) andhydroxyapatite(Sharma et al., 2019).

In recent years, mesoporous silica nanoparticles (MSN) have shown great potential in the agricultural field, particularly regarding to the safe application of pesticides.(Kong et al., 2021) MSN exhibits excellent performance with non-toxicity, biocompatibility, and high thermal stability. In addition, the pore size, meso-structural ordering, and shape of MSN can be easily controlled by varying the experimental conditions during the synthesis.

Various systems based on MSN were studied for the controlled release of different pesticides.(Cao et al., 2018; Chen et al., 2020; Xu et al., 2021) Xu et al. (2021) studied the size effect of MSN on the loading and controlled release of pyraoxystrobin. They found that the loading content increased as the particle size increased.(Xu et al., 2021) Cao et al. (2018) and Huang et al. (2016) reported the preparation of pyraclostrobin-loaded MSNs.(Cao et al., 2018, 2016) They generated stable systems with good fungicidal activity against the fungus *Phomopsis asparagi*. Chen et al. (2020) prepared a sustained-release formulation of methyl eugenol using Schiff base-modified MSN as carrier.(Chen et al., 2020) Wanyika et al. (2013) prepared MSN loaded with metalaxyl, and the nanoparticles showed slower and sustained release of metalaxyl compared to the free fungicide.(Wanyika, 2013) Popat et al. (2012) studied the loading and release of imidacloprid on MSN.(Popat et al., 2012) The results showed that both the type of

mesoporous structure and the surface area of the particles affected the adsorbed amount and the release profile of the pesticide. Meanwhile, abamectin-loaded MSN demonstrated remarkable performance improving photostability, water solubility and bioavailability of the active ingredient.(Feng et al., 2020) Also, the cytotoxicity and antibacterial activity of tebuconazole were improved when MSN was used as nanocarriers.(Murguia et al., 2014) As far as the authors are concerned, the study of MSN and silica-based microparticles for the encapsulation and controlled release of atrazine has not been reported yet.

The objective of this work is to study the synthesis and application of silica-based nano- and microparticles with different porous structures for the controlled release of atrazine in order to decrease the potentially harmful effects of atrazine in the environment. The morphology and particle size were studied by optical microscopy and SEM, and the surface charges by ζ-potential determinations. The encapsulation efficiency and *in vitro* release profiles of the herbicide were evaluated in water. Finally, the phytotoxicity of atrazine was studied by analyzing the Germination Index (GI) and Elongation Root (ER) of *Lactuca sativa* seeds.

2. Experimental work

1. Materials

Tetraethoxysilane (TEOS) (Fluka, Seelze, Alemania), cetyl trimethyl ammonium bromide (CTAB) (Sigma-Aldrich, St. Louis, MO, USA), atrazine commercial formulation (≥90%, Syngenta), sodium hydroxide, ammonia solution, ethanol, methanol, acetonitrile and hexane (Cicarelli, Argentina) were purchased and used without further purification. For herbicide quantification, atrazine standards (98%, Chem Service Inc. USA) were used. Ultrapure water (0.055 μS/cm) obtained in an OSMOION purification unit was used.

2. Preparation of silica-based particles

1. Synthesis of silica nanoparticles

Silica nanoparticles (NP) were synthesized by a modified Stöber method.(Kadhem et al., 2018; Stöber et al., 1968) Briefly, 200 mL of ethanol and 22 mL of ammonia were mixed in a round bottom flask and stirred at 300 rpm. Then, 14 mL of TEOS were quickly added and the mixture was allowed to react for 12 h. In order to eliminate the remaining reactants, nanoparticles were centrifuged and re-dispersed five times in distilled water.

2. Synthesis of mesoporous silica nanoparticles

MCM-41 type mesoporous silica nanoparticles (MSN) were synthesized following the methodology reported by William et al.(Williams et al., 2015) First, a mixture of 384 mL of water (21 mol), 2.8 mL of a 2 M sodium hydroxide (5.6 mmol) solution and 800 mg of CTAB (2.2 mmol) was prepared. Then, 4 mL TEOS (18 mmol) was added dropwise to the mixture and the solution was stirred for 2 h at 80 °C. After cooling to room temperature, the particles were filtered, washed with water to a neutral pH and dried at 60 °C. Finally, the particles were calcined for 4 h at 550 °C in order to remove the remained surfactant.

3. *Synthesis of nanostructured microparticles (M-MSN and M-NP)*

Nanostructured microparticles were prepared using a w/o emulsion technique. First, 0.5 mL of a hydroalcoholic (1:1) suspension of nanoparticles (MSN or NP) at a concentration of 6.5 % w/v was added dropwise to 100 mL of sunflower oil stirred at 250, 300 and 400 rpm and heated in a water bath at 40 °C for 4 h. The suspension was left at room temperature in order to allow the decantation of the microparticles. Then, the oil was removed and the microparticles were washed 3 times with hexane. Finally, microparticles conformed by MSN or NP (M-MSN and M-NP, respectively) were calcined 4 h at 550°C.

3. Nano- and microparticles characterization

4. *Particle size and morphology*

Nanoparticle size distribution was measured by dynamic light scattering (DLS) using BI-200SM equipment (Brookhaven). The measures were performed using a detection angle of 90º and at a temperature of 30 ºC. With the aim of minimizing the noise to signal ratio, an appropriate dilution of samples was carried out with filtered ultrapure water.

The morphology of nano- and microparticles was studied by SEM. Samples were put over an aluminum stub and sputter-coated with gold using a Balzer SCD 030 sputter coater at 40 mA during 90 s. All the samples were examined using an acceleration voltage of 3 kV in a ZEISS FE-SEM Σigma microscope (Jena, Germany).

The mesoporous structure of the nanoparticles was examined by transmission electron microscopy (TEM). Particles were placed on a carbon-coated copper grid, air-dried and viewed using a JEOL-2100 Plus electron microscope (JEOL, Tokyo, Japan) at an accelerating voltage of 200 kV.

Microparticles were also observed in an optical microscope (DM 2500 M, Leica, Germany) coupled with a camera (DFC 290 HD, Leica). The mean particle diameter was

determined using image processing software (ImageJ, National Institutes of Health, Bethesda, Maryland, USA), after analyzing approximately 300 particles per sample.

5. ζ potential

ζ potential measurements were carried out at neutral pH using Zetasizer Nano-series Malvern (ZS90) equipment. Suspensions of N and MSN (1 g L^{-1}) were prepared in deionized water and sonicated for 10 min.

6. Fourier transform infrared spectroscopy (FTIR)

FTIR spectra of particles were obtained using a Shimadzu Model 8201 (Tokyo, Japan) Fourier transform spectrophotometer in the frequency range between 400–4000 cm^{-1} (spectral resolution: 4 cm^{-1}, number of scans: 60). Samples (approximately 2 mg) were mixed with 100 mg of dry KBr (potassium bromide) and the mixtures were then grounded into a fine powder before compressing into a disc.

7. Surface area and porosity of MSN

The textural properties were performed using nitrogen sorption analyses on a Micromeritics ASAP 2020 Plus sorptometer. The samples were previously degassed at 100 °C overnight. The surface area and average pore diameter measurements were calculated using the Brunauer-Emmett-Teller (BET) and the Barrett-Joyner-Halenda (BJH) models, respectively. The total pore volume was estimated at p/po ~ 0.99. The micropore volume and the specific surface area of the mesopores were calculated with the *t*-plot method in the 3.5 Å < *t* < 5.0 Å range.

8. Atrazine encapsulation efficiency

For atrazine encapsulation, 30 mg of particles (MSN, M-MSN and M-NP) were suspended in 5 mL of a saturated atrazine solution (6.0 mg/mL) in methanol. The mixture was kept under stirring for 24 h, and then the solvent was removed. The atrazine-loaded particles were dried for 4 h at 30 °C. In order to evaluate the encapsulation efficiency,

particles were suspended in ethanol and stirred for 24 h. The herbicide concentration in the supernatant of the suspensions was quantified.

9. Atrazine release assay

Approximately 10 mg of atrazine-loaded particles were dispersed in 20 mL of ultrapure water and the vials were incubated at 25 °C. A dialysis bag (Cellu·Sep T1, nominal MWCO: 3500) was employed to confine nanoparticles for sampling. At different times, 1 mL of sample was taken and replaced with an equal volume of fresh medium. Experiments were performed in duplicate. Atrazine quantification was performed by HPLC employing an HPLC-UV/Visible Waters chromatograph equipped with a YMC-Triart C18 column (5 µm particle size, 4.6 × 250; inner diameter x length) and a Waters 2489 UV–vis detector. The atrazine retention time was 5.32 min. The mobile phase consisted of an acetonitrile/water mixture (70:30 v/v) acidified with acetic acid at a flow rate of 1.0 $mLmin^{-1}$. The column temperature and the detection wavelength were 25 °C and 221 nm, respectively. A calibration curve was performed in the 0–30 mg L^{-1} range. The limit of Detection was 0.3 mg L^{-1} and the Limit of Quantification was 1 mg L^{-1}. LOD and LOQ were determined according to Miller and Miller(Miller and Miller, 2010).

10. Phytotoxicity assays

Phytotoxicity assays were evaluated using an acute toxicity assay according to IRAM 29,114 (IRAM (2008) Norma 29114, n.d.) and EPA 840.4200(EPA, 1996) with slight modifications. A filter paper disc was placed at the bottom of each dish (9.1 cm of diameter). 4 mL of particles dispersion or free atrazine solution in water were added and twenty seeds of the target species (*Lactuca sativa*) were sown in each Petri dish. In all experiments, a concentration of atrazine equivalent to 50 ppm was used in order to emulate an application rate of 2 kg ha^{-1}, which correspond to the recommended dose in the field. In addition**,** distilled water was used as a control. The samples were run in

triplicate. After a period of 3 days, the number of germinated roots and their length was evaluated in terms of the Germination Index (GI) according to Ortega et al (Ortega et al., 2000) and the Elongation Root (RE) with equations (1) and (2).

$$GI = \left(\frac{G}{G_c}\right) \times \left(\frac{RL}{RL_c}\right) \times 100 \quad (1)$$

$$RE = (RL - RL_c) / RL_c \quad (2)$$

where G is the number of germinated seeds in the sample, G_c is the number of germinated in the control, RL is the average root length in the sample and RL_c is the average root length in the control. GI and RE were analyzed according to, Zucconi,et al.and Bagur-Gonzalez et al.(Bagur-González et al., 2011; Zucconi et al., 1985) respectively.

4. Results and discussion

Table 1 shows the size and ζ potential measurements of MSN and microparticles based on MSN and NP. The average size of MSN was higher than NP (304 ± 35 vs 192 ±17 nm). These differences are also reflected in SEM micrographs (Figure 1.a and d.).

Table 1. Particle size and surface charge of silica-based nano- and microparticles

	Particle size	ζ potential (mV)
NP	192 ±17 nm	-49.90 (±1.50)
MSN	304 ± 35 nm	-36.20 (±1.15)
M-MSN	158 ± 25 µm	-
M-NP	147 ± 32 µm	-

The ζ potential of NP indicates a higher negative surface charge in comparison with mesoporous particles (-49.90 ± 1.50 vs -36.20 ± 1.15 mV), which may be attributed to higher condensation of silanol groups to siloxanes during the calcination step after MSN synthesis.[16]

MSN microstructure was examined by transmission electron microscopy (Figure 1.g and h). Obtained micrographs show a highly ordered periodic structure porous microstructure. Similar structures were reported by Cai et al. for MCM-41 nanoparticles.(Cai et al., 2001)

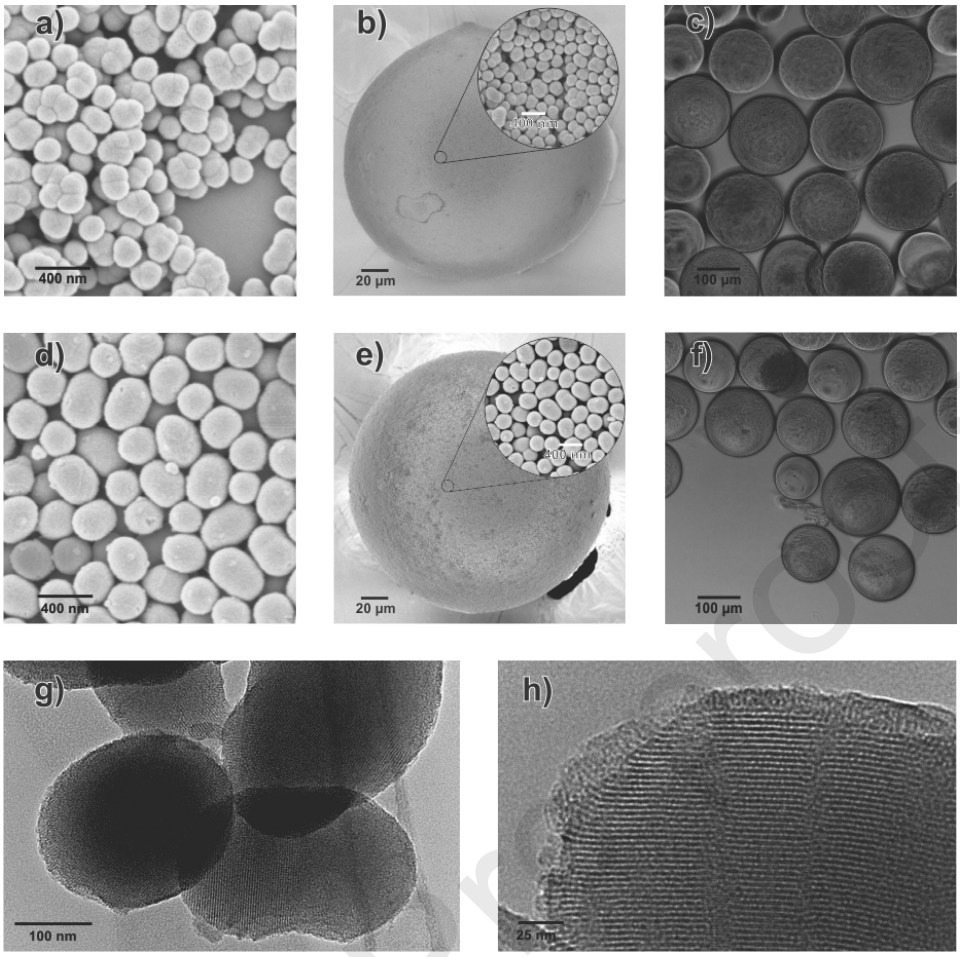

Figure 1. SEM micrograph of NP (a), M-NP (b), MSN (d) and M-MSN (e). Optical microscope images of M-NP (c) and M-MSN (f). TEM images of MSN (g and h).

The influence of stirring rate on microparticle size is displayed in Figure 2. At 200 rpm, particles sizes of 202 ± 49 µm were obtained. At higher stirring rates (250 and 400 rpm), smaller particles of similar size were obtained (147 ± 29 and 147 ± 32 µm). The morphology of microparticles formed by NP at a stirring rate of 400 rpm (M-NP) are shown in Figure 1.b and c. A spherical geometry and smooth surface is observed, with a diameter of approximately 150 µm (Table 1). Similar results were obtained for M-MSN particles (Figure 1.e and f). It is noteworthy to mention that the proposed microparticles synthesis technique has not yet been reported.

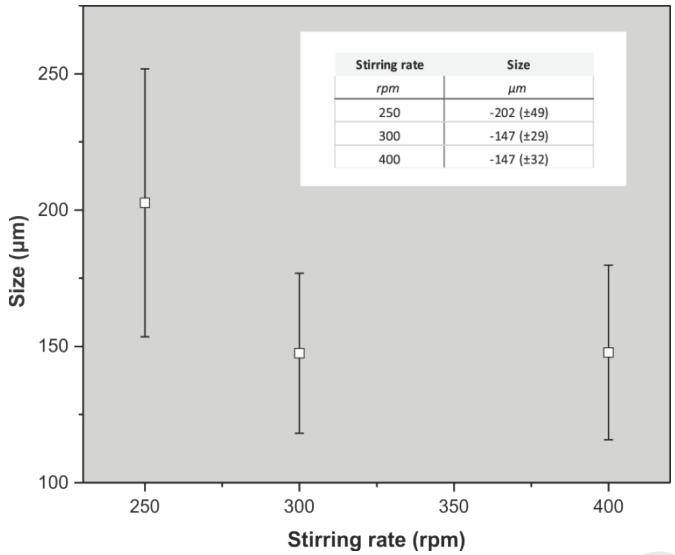

Figure 2. Influence of stirring rate in the size of M-NP.

Figure 3 shows the isotherm (a) and the pore size distribution (b) for MSN particles.

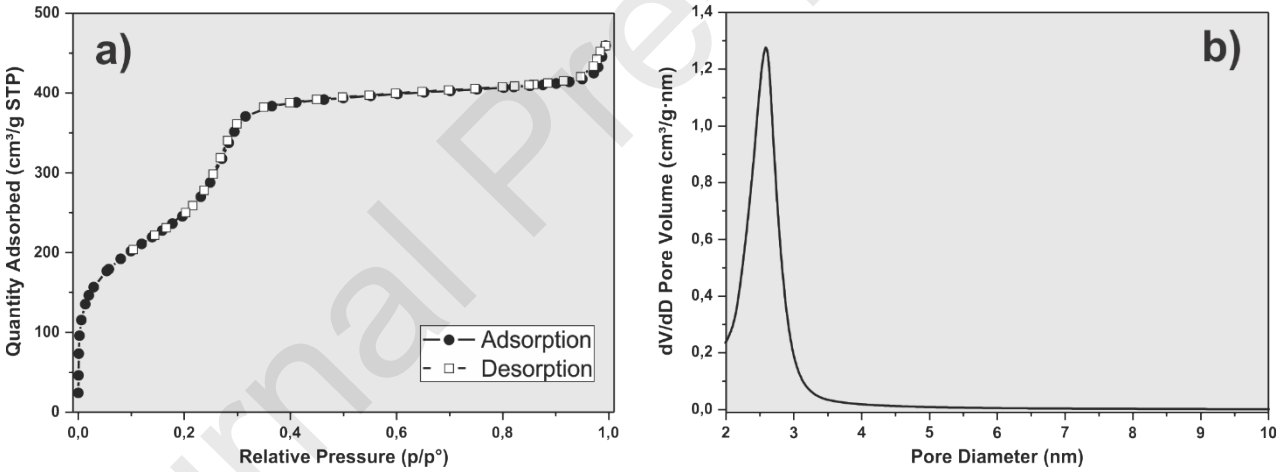

Figure 3. Adsorption and desorption isotherm (a) and pore size distribution (b) of MSN particles.

In Figure 3.a, it can be observed that MSN exhibits a Type IV adsorption isotherm, typically for samples with mesoporosity. Type IV isotherms are associated with capillary condensation in mesopores, characterized by the steep slope at higher relative pressures. The initial part of the Type IV isotherm follows the same path as the Type II. Textural properties of MSN are shown in Table 2.

Table 2. Textural properties of MSN.

BET specific surface area	(m^2/g)	1143
Micropore specific surface area	(m^2/g)[a]	0
Mesopore specific surface area	(m^2/g)	1143
Total pore volume	(cm^3/g)	0.699
Micropore volume	(cm^3/g)	0
Mesopore volume	(cm^3/g)[a]	0.699
Average mesopore diameter	(nm)	2.87

[a]Micropore surface area = BET specific surface area – Mesopore surface area.

Mesopore volume = Total pore volume – Micropore volume.

Note that MSN is a completely mesoporous material. The results obtained are in agreement with TEM images reported in the current work and are similar that the values reported in the literature. (Ning et al., 2019)

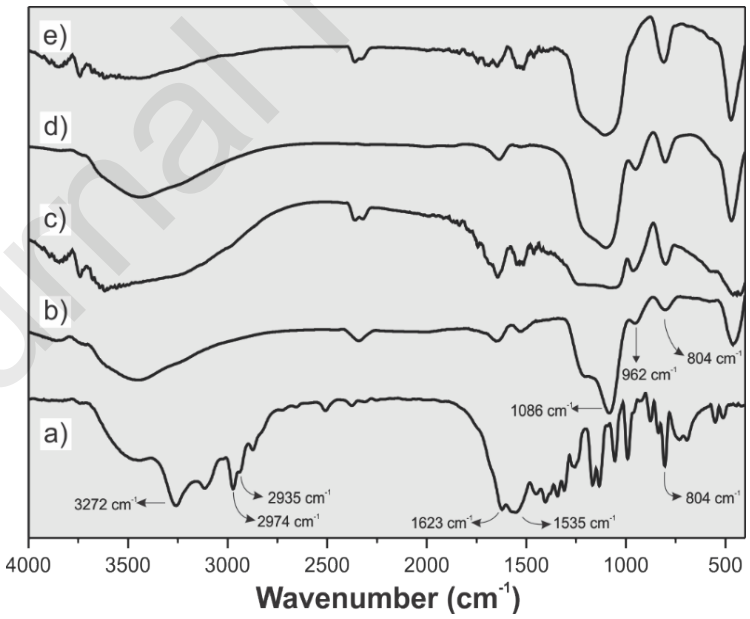

Figure 4. FTIR spectra of atrazine (a), MSN (b), MSN-atz (c), NP (d) and M-NP-atz (e).

FTIR spectra of atrazine and the particle systems are shown in Figure 4. The spectra obtained for MSN, MSN-atz, NP and M-NP-atz (Figure 4.b, c, d and e) show an absorption peak at 800 cm^{-1} and a broad intensity band at 1086 cm^{-1} assigned to Si-O-Si symmetric and asymmetric stretching respectively. A low-intensity peak corresponding to Si-OH stretching is present at 962 cm^{-1}.(Cuesta Zapata et al., 2016; Serrano et al., 2018) The FTIR spectrum of atrazine (Figure 4.a) exhibited a band at 3272 cm^{-1} which is attributed to the amine groups, while bands at 2974 and 2935 cm^{-1} were assigned to CH_3 and CH groups stretching vibrations.(Czaplicka et al., 2018) The stretching vibrations of the 1,3,5-triazine ring appeared at 1623 and 1535 cm^{-1}. Several bands from 1450 to 1300 cm^{-1} were observed due to deformation vibrations of this ring. In addition, stretching vibrations of C–Cl groups were observed 804 cm^{-1}. The encapsulation of the herbicide is confirmed by the presence of the characteristic absorption band at 804 cm^{-1} in MSN-atz and M-NP-atz spectra (Figures 4.c and e).

Table 3. Encapsulation efficiency of MSN, M-MSN and M-NP.

	Encapsulation efficiency *mg atrazine/100 mg particles*
MSN	5.41 ± 0.53
M-MSN	3.21 ± 0.28
M-NP	3.42 ± 0.84

The results of atrazine encapsulation efficiency are shown in Table 3. This parameter could be driven by different aspects such as particle porosity and superficial charge. Among the studied systems, MSN presented higher encapsulation efficiency (5.41 ± 0.53 mg/100 mg particles). Considering that microparticles are formed by nanoparticles aggregation, MSN exhibits lower diffusive limitations. Even though MSN have greater porosity than NP, M-MSN and M-NP showed similar encapsulation

efficiency (3.21 ± 0.28 and 3.42 ± 0.84 mg/100 mg particles, respectively). Similar results were obtained for different drugs with low water solubility entrapped into mesoporous silica nanoparticles.(Moodley and Singh, 2021; Popat et al., 2012; Xu et al., 2021) This effect could be explained by the higher superficial charge in NP, which increases particle-atrazine interaction.

In agriculture, the use of sustained-release systems could offer a longer duration of action of the pesticide in comparison with traditional methods. This may reduce the number of pesticide applications required and enhance targeting, lowering the detrimental effects of excessive pesticide concentrations in the environment.(Busatto et al., 2019)

Release assays in water media were carried out to investigate the effect of particle morphology on atrazine release profiles (Figure 5). The results showed differences between the proposed delivery systems. Particles formed by mesoporous structures (MSN and M-MSN) showed sustained release for at least 24 h. MSN showed a higher percentage of herbicide released than M-MSN (approximately 70% vs. 50%, respectively) and a slower release rate. This could be explained by the greater tortuosity and higher limitations to mass transfer present in the microparticles. In contrast, M-NP showed a higher atrazine release rate due to the non-porous structure of the NP based microparticles, reaching a plateau after 10 h. Also, a lower percentage of drug release (30% of the loaded atrazine) was observed in the period studied, which is attributed to higher atrazine-nanoparticle interaction and to diffusive limitations related to non-porous NP.

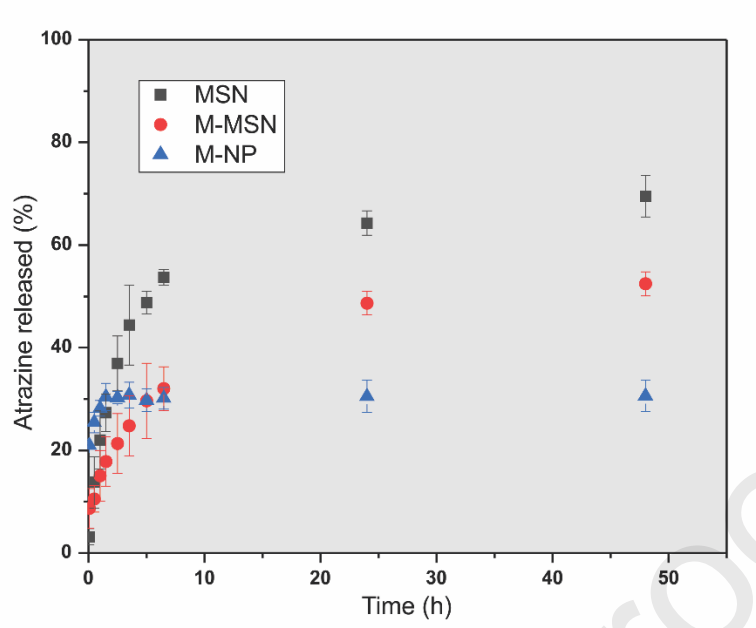

Figure 5. Atrazine release from MSN, M-MSN and M-NP.

In order to study mechanism release, the obtained release data of MSN and M-MSN was analyzed using three mathematical model: zero order, first order and Higuchi. Model parameters were calculated using Solver tool included in the software Excel 365. Release values lower than $M/M_\infty < 0{,}6$ (where M is the drug release at a certain time and M_∞ is the total drug release) were used for model fit. The performance of the obtained model was evaluated with the regression coefficients R^2 and AIC (Akaike information criteria) (eq.3).

$$AIC = n_c.\ln(SSR) + 2p \quad \text{(eq. 3)}$$

where n_c is the number of dissolution points, SSR is the weight sum of square of residues and p is the number of parameters of the model.(Simionato et al., 2018)

Table 4 shows the values of R^2 and AIC of the four model for MSN and M-MSN. Higuchi model showed better performance among the studied models (greater R^2 and lower AIC).

Table 4. Kinetics models parameter obtained for atrazine release from MSN and M-MSN.

Model	Statistics	MSN	M-MSN
Zero Order	*K*	0.14	-0.166
	r^2	0.884	0.873
	AIC	-15.952	-16.68
First Order	*K*	0.288	0.190
	r^2	0.968	0.780
	AIC	-34.077	-23.056
Higuchi	*K*	0.317	0.254
	r^2	**0.988**	**0.961**
	AIC	**-43.534**	**-38.603**

This results suggest that atrazine release from both studied platforms is a square root time-dependent process governed by Fickian diffusion.(Basak et al., 2008; Costa and Sousa Lobo, 2001; Ortiz-Islas et al., 2021)

Finally, atrazine encapsulated phytotoxicity results are shown in Table 5.

Table 5. Phytotoxicity RE and GI parameters for free atrazine and encapsulated in MSN and M-MSN.

	RE	GI
MSN	-0.086	83.784
M-MSN	-0.040	77.911
Free atrazine	-0.616	32.576

Germination is the first step of material exchange between the environment and the developing plant. The root elongation bioassay is one of the most commonly used test methods for environmental monitoring in terms of simplicity, rapidity and economy.(Park et al., 2016) In this study, the number of germinated seeds and the root elongation are measured as sensible parameters for phytotoxicity testing.(Bagur-González et al., 2011; Busatto et al., 2019) A phytotoxicity test was performed using *Lactuca sativa* seeds to

evaluate the effects of atrazine encapsulation on its phytotoxicity. GI and RE parameters provide information on the phytotoxicity of a compound compared to a control (ultrapure water). RE can take values ranging from -1 to greater than 0, higher RE values represent lower phytotoxicity of the evaluated system.

According to Bagur et al. a phytotoxicity scale could be established as follows: 0 to -0.25, low; -0.25 to -0.5, moderate; -0.5 to -0.75, high and -0.75 to 1, very high toxicity. RE greater than 0 would indicate hormesis (stimulation of the growth of the seed).(Bagur-González et al., 2011)

The results obtained for the developed particles showed differences between free atrazine or encapsulated in MSN or M-MSN. The RE value obtained for the free herbicide evidence a high phytotoxicity (RE = -0.616). In contrast, RE values MSN and M-MSN (-0.086 and -0.040, respectively) demonstrated that phytotoxicity of atrazine was attenuated when encapsulated in the developed mesoporous nanoparticles. GI results are in agreement with those obtained for RE, where MSN and M-MSN showed higher values than free atrazine (83.784 and 77.991 vs. 32.576). Indeed, GI showed that the MSN and M-MSN systems did not present phytotoxicity (GI higher than 60%).

Conclusions

Silica nanoparticles (NP and MSN) were synthetized and evaluated as atrazine delivery systems. In addition, a novel method for producing nanostructured microparticles (M-NP and M-MSN) using a w/o emulsion technique is presented. MSN showed a highly ordered microstructure with a high specific area (1143 g/cm^2). Atrazine was encapsulated in the different particles, obtaining higher efficiencies for MSN. Release profiles obtained for MSN and M-MSN fitted very well with Higuchi model, suggesting that atrazine release from these particles is governed by Fickian diffusion. In addition, the encapsulation of the studied herbicide in MSN and M-MSN decreased its phytotoxicity compared with free atrazine. Further investigations will consider the application of developed microparticles in agrochemicals encapsulation and catalyst supports. Overall, the results showed that MSN could control atrazine release and reduce the herbicide phytotoxicity.

Acknowledgements

We acknowledge the financial support from CONICET, MINCyT, UTN and UNL.

5. References

Andrade, L.L. de, do Espirito Santo Pereira, A., Fernandes Fraceto, L., Bueno dos Reis Martinez, C., 2019. Can atrazine loaded nanocapsules reduce the toxic effects of this herbicide on the fish Prochilodus lineatus? A multibiomarker approach. Sci. Total Environ. 663, 548–559. https://doi.org/10.1016/J.SCITOTENV.2019.01.380

Bagur-González, M.G., Estepa-Molina, C., Martín-Peinado, F., Morales-Ruano, S., 2011. Toxicity assessment using Lactuca sativa L. bioassay of the metal(loid)s As, Cu, Mn, Pb and Zn in soluble-in-water saturated soil extracts from an abandoned mining site. J. Soils Sediments 11, 281–289. https://doi.org/10.1007/s11368-010-0285-4

Basak, S.C., Kumar, K.S., Ramalingam, M., 2008. Design and release characteristics of sustained release tablet containing metformin HCl. Rev. Bras. Ciencias Farm. J. Pharm. Sci. 44, 477–483. https://doi.org/10.1590/S1516-93322008000300018

Busatto, C.A., Taverna, M.E., Lescano, M.R., Zalazar, C., Estenoz, D.A., 2019. Preparation and Characterization of Lignin Microparticles-in-Alginate Beads for Atrazine Controlled Release. J. Polym. Environ. 27, 2831–2841. https://doi.org/10.1007/s10924-019-01564-2

Cai, Q., Luo, Z.S., Pang, W.Q., Fan, Y.W., Chen, X.H., Cui, F.Z., 2001. Dilute solution routes to various controllable morphologies of MCM-41 silica with a basic medium. Chem. Mater. 13, 258–263. https://doi.org/10.1021/cm990661z

Cao, L., Zhang, H., Cao, C., Zhang, J., Li, F., Huang, Q., 2016. Quaternized Chitosan-Capped Mesoporous Silica Nanoparticles as Nanocarriers for Controlled Pesticide Release. Nanomater. 2016, Vol. 6, Page 126 6, 126. https://doi.org/10.3390/NANO6070126

Cao, L., Zhang, H., Zhou, Z., Xu, C., Shan, Y., Lin, Y., Huang, Q., 2018. Fluorophore-free luminescent double-shelled hollow mesoporous silica nanoparticles as pesticide

delivery vehicles. Nanoscale 10, 20354–20365. https://doi.org/10.1039/C8NR04626C

Chen, H., Chen, L., Shen, Z., Zhou, H., Hao, L., Xu, H., Zhou, X., 2020. Synthesis of mesoporous silica post-loaded by methyl eugenol as an environment-friendly slow-release bio pesticide. Sci. Reports 2020 101 10, 1–12. https://doi.org/10.1038/s41598-020-63015-6

CHEN, X. ting, Wang, T., 2019. Preparation and characterization of atrazine-loaded biodegradable PLGA nanospheres. J. Integr. Agric. 18, 1035–1041. https://doi.org/10.1016/S2095-3119(19)62613-4

Chevillard, A., Angellier-Coussy, H., Guillard, V., Gontard, N., Gastaldi, E., 2012. Controlling pesticide release via structuring agropolymer and nanoclays based materials. J. Hazard. Mater. 205–206, 32–39. https://doi.org/10.1016/J.JHAZMAT.2011.11.093

Clemente, Z., Grillo, R., Jonsson, M., Santos, N.Z.P., Feitosa, L.O., Lima, R., Fraceto, L.F., 2014. Ecotoxicological evaluation of poly(epsilon-caprolactone) nanocapsules containing triazine herbicides. J. Nanosci. Nanotechnol. 14, 4911–4917. https://doi.org/10.1166/JNN.2014.8681

Costa, P., Sousa Lobo, J.M., 2001. Modeling and comparison of dissolution profiles. Eur. J. Pharm. Sci. 13, 123–133. https://doi.org/10.1016/S0928-0987(01)00095-1

Cuesta Zapata, P.M., Nazzarro, M.S., Gonzo, E.E., Parentis, M.L., Bonini, N.A., 2016. Cr/SiO2 mesoporous catalysts: Effect of hydrothermal treatment and calcination temperature on the structure and catalytic activity in the gas phase dehydration and dehydrogenation of cyclohexanol. Catal. Today 259, 39–49. https://doi.org/10.1016/j.cattod.2015.04.038

Czaplicka, M., Barchanska, H., Jaworek, K., Kaczmarczyk, B., 2018. The interaction

between atrazine and the mineral horizon of soil: a spectroscopic study. J. Soils Sediments 18, 827–834. https://doi.org/10.1007/s11368-017-1843-9

de Albuquerque, F.P., de Oliveira, J.L., Moschini-Carlos, V., Fraceto, L.F., 2020. An overview of the potential impacts of atrazine in aquatic environments: Perspectives for tailored solutions based on nanotechnology. Sci. Total Environ. 700, 134868. https://doi.org/10.1016/J.SCITOTENV.2019.134868

De Oliveira, J.L., Campos, E.V.R., Gonçalves Da Silva, C.M., Pasquoto, T., Lima, R., Fraceto, L.F., 2015. Solid lipid nanoparticles co-loaded with simazine and atrazine: preparation, characterization, and evaluation of herbicidal activity. J. Agric. Food Chem. 63, 422–432. https://doi.org/10.1021/JF5059045

EPA, 1996. Ecological effects test guidelines. Seed germination/root elongation toxicity test OPPTS 850:4200.

Feng, J., Chen, W., Shen, Y., Chen, Q., Yang, J., Zhang, M., Yang, W., Yuan, S., 2020. Fabrication of abamectin-loaded mesoporous silica nanoparticles by emulsion-solvent evaporation to improve photolysis stability and extend insecticidal activity. Nanotechnology 31, 345705. https://doi.org/10.1088/1361-6528/ab91f0

Fernández-Pérez, M., Flores-Céspedes, F., González-Pradas, E., Villafranca-Sánchez, M., Pérez-García, S., Garrido-Herrera, F.J., 2004. Use of Activated Bentonites in Controlled-Release Formulations of Atrazine. J. Agric. Food Chem. 52, 3888–3893. https://doi.org/10.1021/JF030833J

Grillo, R., Pereira, A. do E.S., de Melo, N.F.S., Porto, R.M., Feitosa, L.O., Tonello, P.S., Filho, N.L.D., Rosa, A.H., Lima, R., Fraceto, L.F., 2011. Controlled release system for ametryn using polymer microspheres: Preparation, characterization and release kinetics in water. J. Hazard. Mater. 186, 1645–1651. https://doi.org/10.1016/J.JHAZMAT.2010.12.044

IRAM (2008) Norma 29114, n.d. Método de ensayo de toxicidad aguda con semillas de lechuga (Lactuca sativa L.). Método Papel. Calid. Ambient. - Métodos Biológicos.

Jain, S.K., Dutta, A., Kumar, J., Shakil, N.A., 2020. Preparation and characterization of dicarboxylic acid modified starch-clay composites as carriers for pesticide delivery. Arab. J. Chem. 13, 7990–8002. https://doi.org/10.1016/J.ARABJC.2020.09.028

Kadhem, A., Xiang, S., Nagel, S., Lin, C.-H., Fidalgo de Cortalezzi, M., 2018. Photonic Molecularly Imprinted Polymer Film for the Detection of Testosterone in Aqueous Samples. Polymers (Basel). 10, 349. https://doi.org/10.3390/polym10040349

Kong, X., Zhang, B., Wang, J., 2021. Multiple Roles of Mesoporous Silica in Safe Pesticide Application by Nanotechnology: A Review. J. Agric. Food Chem. 69, 6735–6754. https://doi.org/10.1021/acs.jafc.1c01091

Małyszka, T., Jankowski, T., 2004. Controlled release formulations of atrazine produced by tumbling agglomeration. J. Plant Prot. Res. 44, 221–230.

Miller, J.N., Miller, J.C., 2010. Statistics and Chemometrics for Analytical Chemistry Sixth edition, 6th ed. Pearson, Harlow.

Moodley, T., Singh, M., 2021. Polymeric mesoporous silica nanoparticles for combination drug delivery in vitro. Biointerface Res. Appl. Chem. 11, 11905–11919. https://doi.org/10.33263/BRIAC114.1190511919

Murguia, J.R., Mas, N., Galiana, I., Hurtado, S., Mondragon, L., Bernardos, A., Sancenon, F., Amoros, P., Abril-Utrillas, N., Marcos, D., Martinez-Manez, R., 2014. Enhanced antifungal efficacy of tebuconazole using gated pH-driven mesoporous nanoparticles. Int. J. Nanomedicine 9, 2597. https://doi.org/10.2147/IJN.S59654

Narenderan, S.T., Meyyanathan, S.N., Babu, B., 2020. Review of pesticide residue analysis in fruits and vegetables. Pre-treatment, extraction and detection techniques. Food Res. Int. 133, 109141. https://doi.org/10.1016/J.FOODRES.2020.109141

Ning, C., Jiajia, J., Meng, L., Hongfei, Q., Xianglong, W., Tingli, L., 2019. Electrophoretic deposition of GHK-Cu loaded MSN-chitosan coatings with pH-responsive release of copper and its bioactivity. Mater. Sci. Eng. C 104, 109746. https://doi.org/10.1016/J.MSEC.2019.109746

Ortega, M.C., Aguado, M.T., Moreno, M.T., 2000. Propuesta de Bioensayos para detectar factores fitotóxicos en sustratos y enmiendas. Actas Hortic. 32, 363–376.

Ortiz-Islas, E., Sosa-Arróniz, A., Manríquez-Ramírez, M.E., Rodríguez-Pérez, C.E., Tzompantzi, F., Padilla, J.M., 2021. Mesoporous silica nanoparticles functionalized with folic acid for targeted release Cis-Pt to glioblastoma cells. Rev. Adv. Mater. Sci. 60, 25–37. https://doi.org/10.1515/RAMS-2021-0009/MACHINEREADABLECITATION/RIS

Park, J., Yoon, J. hyun, Depuydt, S., Oh, J.W., Jo, Y. min, Kim, K., Brown, M.T., Han, T., 2016. The sensitivity of an hydroponic lettuce root elongation bioassay to metals, phenol and wastewaters. Ecotoxicol. Environ. Saf. 126, 147–153. https://doi.org/10.1016/j.ecoenv.2015.12.013

Pereira, A.E.S., Grillo, R., Mello, N.F.S., Rosa, A.H., Fraceto, L.F., 2014. Application of poly(epsilon-caprolactone) nanoparticles containing atrazine herbicide as an alternative technique to control weeds and reduce damage to the environment. J. Hazard. Mater. 268, 207–215. https://doi.org/10.1016/J.JHAZMAT.2014.01.025

Popat, A., Liu, J., Hu, Q., Kennedy, M., Peters, B., Lu, G.Q. (Max), Qiao, S.Z., 2012. Adsorption and release of biocides with mesoporous silica nanoparticles. Nanoscale 4, 970–975. https://doi.org/10.1039/C2NR11691J

Runes, H.B., Bottomley, P.J., Lerch, R.N., Jenkins, J.J., 2001. Atrazine remediation in wetland microcosms. Environ. Toxicol. Chem. 20, 1059–1066. https://doi.org/10.1002/etc.5620200517

Serrano, M.R., María, A., Gramaglia, P., 2018. Síntesis de sílice mesoestructurada : determinación de las condiciones óptimas de extracción del templato Synthesis of ordered mesoporous silica : determination of optimum conditions for template removal.

Sharma, P., Rohilla, D., Chaudhary, S., Kumar, R., Singh, A.N., 2019. Nanosorbent of hydroxyapatite for atrazine: A new approach for combating agricultural runoffs. Sci. Total Environ. 653, 264–273. https://doi.org/10.1016/j.scitotenv.2018.10.352

Simionato, L.D., Petrone, L., Baldut, M., Bonafede, S.L., Segall, A.I., 2018. Comparison between the dissolution profiles of nine meloxicam tablet brands commercially available in Buenos Aires, Argentina. Saudi Pharm. J. 26, 578–584. https://doi.org/10.1016/j.jsps.2018.01.015

Stöber, W., Fink, A., Bohn, E., 1968. Controlled growth of monodisperse silica spheres in the micron size range. J. Colloid Interface Sci. 26, 62–69. https://doi.org/10.1016/0021-9797(68)90272-5

Taverna, M.E., Busatto, C.A., Lescano, M.R., Nicolau, V.V., Zalazar, C.S., Meira, G.R., Estenoz, D.A., 2018. Microparticles based on ionic and organosolv lignins for the controlled release of atrazine. J. Hazard. Mater. 359, 139–147. https://doi.org/10.1016/j.jhazmat.2018.07.010

Touloupakis, E., Margelou, A., Ghanotakis, D.F., 2011. Intercalation of the herbicide atrazine in layered double hydroxides for controlled-release applications. Pest Manag. Sci. 67, 837–841. https://doi.org/10.1002/PS.2121

Wanyika, H., 2013. Sustained release of fungicide metalaxyl by mesoporous silica nanospheres. Nanotechnol. Sustain. Dev. First Ed. 321–329. https://doi.org/10.1007/978-3-319-05041-6_25

Williams, S., Neumann, A., Bremer, I., Su, Y., Dräger, G., Kasper, C., Behrens, P., 2015.

Nanoporous silica nanoparticles as biomaterials: evaluation of different strategies for the functionalization with polysialic acid by step-by-step cytocompatibility testing. J. Mater. Sci. Mater. Med. 26. https://doi.org/10.1007/s10856-015-5409-3

Xu, Y., Xu, C., Huang, Q., Cao, L., Teng, F., Zhao, P., Jia, M., 2021. Size effect of mesoporous silica nanoparticles on pesticide loading, release, and delivery in cucumber plants. Appl. Sci. 11, 1–15. https://doi.org/10.3390/app11020575

Zucconi, F., Mónaco, A., Forte, M., 1985. Phytotoxins during the stabilization of organic matter. Compost. Agric. other wastes 73–86.

6. Tables

Table 1. Particle size and surface charge of silica-based nano- and microparticles

	Particle size	ζ potential (mV)
NP	192 ±17 nm	-49.90 (±1.50)
MSN	304 ± 35 nm	-36.20 (±1.15)
M-MSN	158 ± 25 µm	-
M-NP	147 ± 32 µm	-

Table 2. Textural properties of MSN.

BET specific surface area	(m^2/g)	1143
Micropore specific surface area	(m^2/g)[a]	0
Mesopore specific surface area	(m^2/g)	1143
Total pore volume	(cm^3/g)	0.699
Micropore volume	(cm^3/g)	0
Mesopore volume	(cm^3/g)[a]	0.699
Average mesopore diameter	(nm)	2.87

[a]Micropore surface area = BET specific surface area – Mesopore surface area.

Mesopore volume = Total pore volume – Micropore volume.

Table 3. Encapsulation efficiency of MSN, M-MSN and M-NP.

	Encapsulation efficiency *mg atrazine/100 mg particles*
MSN	5.41 ± 0.53
M-MSN	3.21 ± 0.28
M-NP	3.42 ± 0.84

Table 4. Kinetics models parameter obtained for atrazine release from MSN and M-MSN.

Model	Statistics	MSN	M-MSN
Zero Order	*K*	0.14	-0.166
	r^2	0.884	0.873
	AIC	-15.952	-16.68
First Order	*K*	0.288	0.190
	r^2	0.968	0.780
	AIC	-34.077	-23.056
Higuchi	*K*	0.317	0.254
	r^2	**0.988**	**0.961**
	AIC	**-43.534**	**-38.603**

Table 5. Phytotoxicity RE and GI parameters for free atrazine and encapsulated in MSN and M-MSN.

	RE	GI
MSN	-0.086	83.784
M-MSN	-0.040	77.911
Free atrazine	-0.616	32.576

7. Figure captions

Figure 1. SEM micrograph of NP (a), M-NP (b), MSN (d) and M-MSN (e). Optical microscope images of M-NP (c) and M-MSN (f). TEM images of MSN (g and h).

Figure 2. Influence of stirring rate in the size of M-NP.

Figure 3. Adsorption and desorption isotherm (a) and pore size distribution (b) of MSN particles.

Figure 4. FTIR spectra of atrazine (a), MSN (b), MSN-atz (c), NP (d) and M-NP-atz (e).

Figure 5. Atrazine release from MSN, M-MSN and M-NP.